Surface Science 129 (1983) 92–106
North-Holland Publishing Company

A LEED DETERMINATION OF THE STRUCTURES OF Ru(001) AND OF CO/Ru(001)-$\sqrt{3} \times \sqrt{3}$ R30°

G. MICHALK

Sonderforschungsbereich 128, Institut für Festkörperphysik, Physik-Department E20, Technische Universität München, D-8046 Garching, Fed. Rep. of Germany

W. MORITZ

Sonderforschungsbereich 128, Institut für Kristallographie und Mineralogie, Universität München, Theresienstrasse 41, D-8000 München 2, Fed. Rep. of Germany

and

H. PFNÜR and D. MENZEL

Sonderforschungsbereich 128, Institut für Festkörperphysik, Physik-Department E20, Technische Universität München, D-8046 Garching, Fed. Rep. of Germany

Received 29 July 1982; accepted for publication 13 March 1983

The structures of Ru(001) and of the $\sqrt{3} \times \sqrt{3}$ R30° overlayer of CO on Ru(001) have been determined by LEED $I-V$ measurements and comparison to calculations. Special attention was paid to accurate angular alignment, selection of a well-ordered portion of the surface, and avoidance of beam-induced changes of the CO layer. Five orders of reflexes over a range of 300 eV each were used for the clean surface and 7 orders over 200 eV each for the CO superstructure. For the clean surface, a slight contraction of the first layer spacing (by 2%) was found which gave r-factors of 0.04 (Zanazzi–Jona) and 0.16 (Pendry) for 5 non-degenerate beams. For the CO structure the most probable geometry is the on-top site with spacings $d(\mathrm{Ru-C}) = 2.0 \pm 0.1$ Å and $d(\mathrm{C-O}) = 1.10 \pm 0.1$ Å ($r_{ZJ} = 0.21$; $r_P = 0.51$). The two threefold hollow and the bridge sites can be clearly excluded.

1. Introduction

The adsorption system CO on the basal Ru(001) surface has been well characterized by a variety of methods (LEED, thermal desorption and work function changes [1–3], XPS and UPS [4], angle-resolved UPS [5], electronic [6] and vibrational [7] electron energy losses as well as IR spectroscopy [8], electron stimulated desorption (ESD) [9] and its angular distribution, ESDIAD [10], and LEED beam profiles [11,12]). Some of these results give indications of the geometry of the adsorbate. The angle-resolved UPS as well as the ESDIAD

0039-6028/83/0000–0000/$03.00

data showed that CO is bound upright, with the C-end attached to the metal; UPS, XPS, IR, and ELS results show that at all coverages only one surface species is present which is best characterized at the optimal development of the $\sqrt{3} \times \sqrt{3}$ R30° (subsequently termed the $\sqrt{3}$ structure) at $\theta = 0.33$ relative to surface Ru atoms and whose properties are changed by lateral interactions below and above this coverage [12,13]. For the $\sqrt{3}$ structure, the vibrational energy [7,8] and the dependence of ESD signals on coverage [9] suggest that the on-top site rather than one of the threefold hollow sites or the twofold bridge is occupied. However, these arguments are weakened by the fact that no new vibrations are seen at high coverages, where at least part of the molecules have to be shifted. A direct determination of the adsorbate geometry appeared desirable, therefore. As the clean surface structure, which has to serve as the point of departure, has not yet been determined either, its determination was undertaken as well.

2. Procedures

2.1. Experimental

For the measurements, a standard stainless steel UHV chamber (base pressure about 1×10^{-10} mbar after bake-out) equipped with four-grid LEED optics with movable Faraday cup, was used. The circular Faraday cup aperture subtended an angle of linear 2.6° (or 1.6×10^{-3} steradians). With a width of the LEED spots of typically 1° (FWHM) over the whole energy range, an integral measurement of intensities was possible. A modification of the LEED gun supply allowed regulated currents as low as 10 nA with a noise below 5%. The ruthenium crystal of purity better than 99.99% was cut by spark erosion, oriented with a Laue camera to less than 0.5° of the (001) plane and mechanically polished with diamond pastes to about 0.25 μm. The resulting crystal was an approximate rectangle of 11×7 mm, 0.8 mm thick. Two short Ta wires, spot-welded to the back of the crystal, were attached to the sample holder. This allowed resistive heating of the sample to 1570 K and cooling down to 100 K with liquid nitrogen. By means of chopping the LEED gun and the sample heating current alternately, direct heating of the sample was possible simultaneously with LEED measurements. In this mode the sample temperature could be kept constant to within 0.1 K using a digital regulator.

The cleaning procedures, which have been described elsewhere [2,3], were monitored using Auger spectroscopy and a fast vibrating capacitor [14]. The latter allowed an accurate measurement of the work function change induced by hydrogen adsorption which has been found [15] to be a sensitive test of absence of carbon impurities which cannot be seen by AES on Ru.

Before the manipulator was inserted into the UHV chamber, the crystal

surface normal and the azimuthal rotation axis were made parallel to within 0.1° by laser reflection. In situ orientation of the sample relative to the beam was possible with the vertical axis of the manipulator head (to 0.1°) and, perpendicular to that axis, with a deflection of the electron beam. To maintain the correct adjustment of the beam for all energies, the chamber had been surrounded with a double mu-metal shield (one each inside and outside) which reduced stray magnetic fields in the beam region to less than 1 μT. The exact orientation of the surface normal parallel to the beam ($\vartheta \equiv 0°$) was determined by checking for the degeneracy of beam $I-V$ profiles as described below.

In order to make sure that a well-ordered part of the surface would be used for the measurements, the crystal reflectivity was mapped by measuring the currents in various LEED beams (0,0; 1,0; 1,1) while shifting the crystal under the beam (diameter about 0.8 mm) in steps of 0.5 mm. An example is shown in fig. 1; the other results were similar. The portion of the surface selected for measurements was inside the 90% area for all examined beams.

The LEED spots of the clean surface exhibited 6mm symmetry at exactly normal incidence which was visibly disturbed by deviations of ϑ as small as 0.1°. This strong angular dependence has been investigated in some detail [16]; an example is displayed in fig. 2. Therefore, even after optimal alignment, the $I-V$ curves of all degenerate spots were measured independently over the whole energy range to detect possible differences in the spectra; only sets with small differences were accepted. The average of these degenerate curves was then used for comparison with the computed spectra. Fig. 3 shows the $I-V$ spectra of the six first order beams together with the averaged curve. It is seen that the averaging reduces the noise.

For optimal ordering of the adsorbed CO in the saturated $\sqrt{3}$ structure, CO was dosed onto the crystal at a pressure of about 2×10^{-8} mbar until

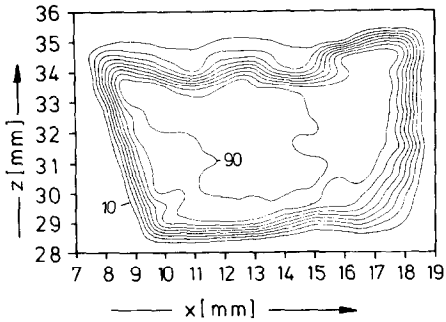

Fig. 1. Example for mapping of the crystal reflectivity with the LEED intensity. Results for the (1, 0) beam at 60 eV and normal incidence are shown; equidensity lines from 90 to 10% in steps of 10% are plotted. The influences of the two support wires (top) and of the thermocouple (bottom, right from centre) can be seen.

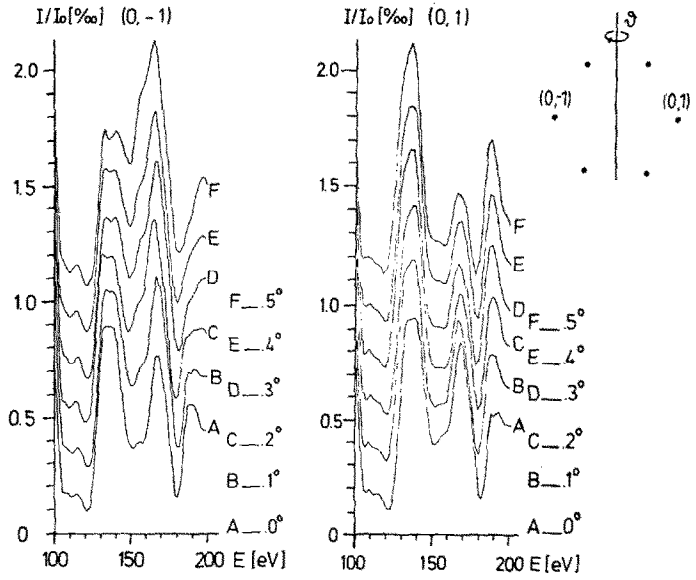

Fig. 2. Example for the dependence of $I-V$ curves of degenerate LEED beams on small angular deviations from normal incidence ((0, −1) and (0, 1) beams; geometry as indicated by inset).

maximum LEED intensity of the (1/3, 1/3) spots was reached, at a sample temperature of 360 K; the crystal was then cooled to 150 K for the $I-V$ measurements. This procedure yielded the optimum superstructure intensity, as checked by various dosing/heating schemes, and reproduced the LEED intensities within 5%.

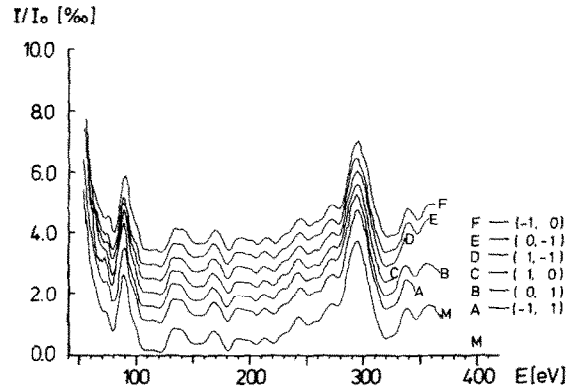

Fig. 3. Example for the agreement of $I-V$ curves of degenerate beams at optimum adjustment, and of the effect of averaging them (lowest curve). Data for the first order beams of clean Ru(001) are shown.

As on many other surfaces, CO adsorbed on Ru(001) is quite sensitive to electron beam damage [1,6,9]. Therefore, special attention was paid to avoiding such disturbances on the $I-V$ results. The beam current was limited to 20 nA for the CO measurements (for the clean surface, 100 nA were used). By checking the time of measurement which would not degrade the superstructure intensity by more than 5%, it was found that detrimental beam effects could be avoided by cleaning and recovering the crystal twice during each energy scan of a single spot. This procedure was adopted in all adsorbate measurements. For both the clean and the covered surface, measurements of all spots observable with the Faraday cup between 40 and 400 eV were carried out. This means 5 orders for the clean and 7 orders for the covered surface. Equivalent beams of the same order were then averaged as described above. The electron energies given are those directly read for the accelerating voltage; no correction for contact potentials was applied as this would have only changed the value of the inner potential.

For further experimental details, see ref. [16].

2.2. *Calculational procedures*

LEED intensity calculations were performed using the RFS scheme and the layer doubling scheme [17] for interlayer scattering. The CO overlayer was treated as a compound layer where the matrix inversion method in angular momentum space was used. The crystal potential for ruthenium was calculated by overlap from free atom potentials using a Slater exchange term with Schwarz's optimized α-parameter [18]. Potentials and phase shifts were calculated relativistically, and in the multiple scattering program spin averaged phase shifts were used [19]. The phase shifts for C and O were taken from a study of CO on Ni(100) by Tong et al. [20], which were also used by Koestner et al. [21] in a study of CO on Rh(111). These potentials have been calculated with an overlap of atomic charge densities between C and Ni and led to an improvement but not to a different result than the use of other potentials. It is not expected that substantial errors are caused in the $I-V$ spectra by using these potentials instead of one which considers the overlap from ruthenium, as the bond lengths are similar for both materials.

Up to eight phase shifts were used, the number depending on energy. The imaginary part of the inner potential, describing the damping of the electron wave, was set energy-dependent to $V_i = 0.85E^{1/3}$ (eV). The real part of the inner potential was chosen to be independent of energy and, as usual, the average value was found by optimizing the r-factor. The optimum value found here for the clean Ru(001) surface is about $V_0 = -12.0$ eV. This value contains the contact potential, as the experimental curves were not corrected for it. Normally, the effective inner potential was not varied in the r-factor analysis for the CO structure, but the calculations for all models were carried out giving

the CO overlayer the same muffin-tin zero as the Ru layer. As a test, a value of 5.5 eV above the Ru muffin-tin zero was used for the CO layer for the calculation for the on-top site. This procedure, which has also been adopted by Andersson and Pendry [22] in a study of CO on Ni(100) and Cu(100), is certainly justified because of the lower electron density between the CO molecules. However, the differences of results for these two V_i values were negligibly small and clearly below the error limit. The bulk value of the Debye temperature for ruthenium, $\theta_D = 410$ K [23], was taken for bulk and surface layers. These non-structural parameters were not varied to find the optimum values since it is often found that surface vibrational amplitudes cannot be derived from such an analysis. The determination of bond lengths and layer spacings is not much influenced by the damping parameter and the Debye temperature, and even different potential approximations lead mostly to the same structural parameters. In a recent study by Nielsen and Adams [24] these influences have been investigated in detail, and the same conclusion was drawn there.

To determine the optimal agreement between experiment and calculation, the r-factors defined by Zanazzi and Jona, r_{ZJ} [25], and by Pendry, r_P [26], have been used. Differences between them will be discussed in connection with the results.

In the basal plane of a hcp structure two possible domains exist: The ABABA... layer sequence can be terminated by an A or a B plane. Both domains are transformed into each other by an additional mirror plane between those of a single domain or by a rotation of 60° (see fig. 4). The existence of both domains causes the 6mm symmetry of the diffraction picture; the single domain has the symmetry 3m. In the models with bridge positions, the single domain contains only a mirror plane, and six domains have to be taken into account. As has been discussed in other studies of basal planes of hcp crystals [27–29] the correct I–V spectra comparable to experiment are obtained by mixing the contributions from all domains. As usual in cases where several domains of a structure exist, this mixing has been done incoherently in the cited works. It can indeed be shown [30] that incoherent averaging is approximately correct as long as the integral intensity of the beams is measured and not the peak intensity. In practice this means that the domain sizes must be large enough and statistically distributed for intensity mixing to be the correct procedure – conditions which are usually given at clean surfaces prepared with standard precision but not always for reconstructed surfaces or adsorbate layers. The average domain size on the same crystal investigated here has been determined in a previous study [31] to be about 50 to 70 atomic distances. This size is large enough to get the whole intensity into the Faraday cup and also to leave multiple scattering effects at the domain boundaries negligibly small. Therefore the contributions of the two possible domains have been averaged incoherently in our calculations.

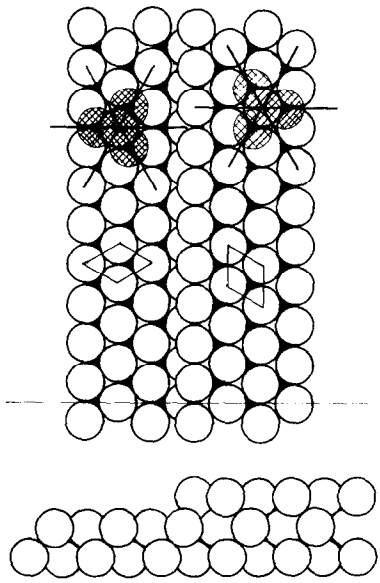

Fig. 4. The two possible domains of a close-packed surface of a hexagonal crystal (top, viewed from above; bottom, side view).

3. Results

3.1. Results for clean Ru(001)

Comparison between experimental and theoretical $I-V$ spectra for clean Ru(001) is shown in fig. 5. The only parameter varied in the calculations is the first layer spacing, d_1. Best agreement is achieved at a small contraction of about 2%, corresponding to $d_1 = 2.10$ Å instead of 2.14 Å, the bulk value. As shown in fig. 6, both r-factors, r_{ZJ} and r_P, lead to the same optimum values for the top layer spacing and the inner potential. The inner potential was taken to be independent of energy and its optimum value is $V_0 = -12.0$ eV. Five non-degenerate beams at normal incidence were used. The minimum averaged r-factors are $\bar{r}_{ZJ} = 0.041$ and $\bar{r}_P = 0.16$. Their dependence on the top layer spacing is shown in figs. 6a and 6b. All single beam r-factors have minima within a range of ± 0.02 Å, and from a statistical analysis, as discussed by Pendry [26], we can estimate an error in d_1 of about the same size. This error, of course, does not include the errors made by the choice of the non-structural parameters, so that the real accuracy may be indeed considerably inferior. The low contraction of the first layer spacing compares well to values found at other close-packed surfaces of hcp crystals [28,29,32,33].

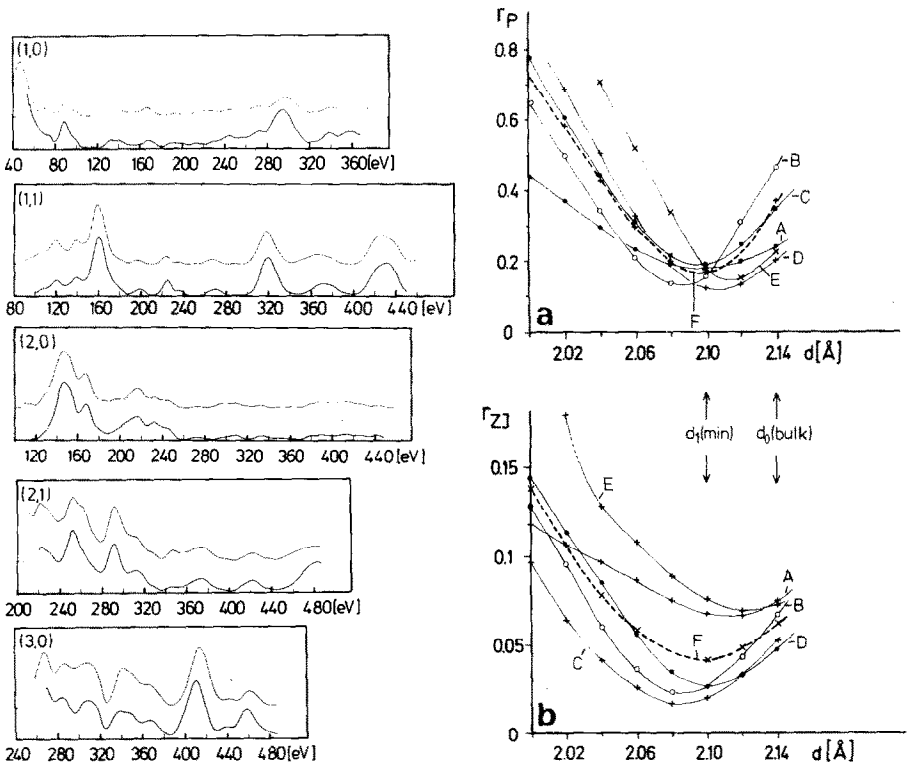

Fig. 5. Comparison of theoretical (for the optimum top spacing of 2.10 Å; top curves) and experimental (bottom curves) $I-V$ spectra for clean Ru(001), for five nondegenerate beams. Experimental curves obtained by averaging over all degenerate beams.

Fig. 6. Dependence of the r-factors according to Zanazzi–Jona, r_{ZJ}, and to Pendry, r_P, on the first layer spacing for clean Ru(001): (A) (1, 0) beam; (B) (1, 1); (C) (2, 0); (D) (2, 1); (E) (3, 0); (F) all beams. The optimum ($\bar{r}_{ZJ} = 0.04$, $\bar{r}_P = 0.16$) is found for $d_1 = 2.10$ Å (bulk value: $d_0 = 2.14$ Å) with $V_0 = -12.0$ eV.

3.2. *Results for the $\sqrt{3}$-CO structure*

As discussed in the introduction, the adsorption of CO on ruthenium has been previously studied by various methods and from these measurements one should expect the CO molecule to be adsorbed with its axis perpendicular to the surface, and in the $\sqrt{3}$ structure it should be bonded to a single ruthenium atom in a linear chain. Nevertheless, to get a clear decision from the analysis of $I-V$ spectra, three other adsorption sites have also been considered: In addition to the on-top position, the CO molecule has been put in the twofold

symmetric bridge position, and above the two possible threefold hollow sites one with a ruthenium atom in the second layer (hcp site) and one with an empty site underneath (fcc site); in each case the CO molecule was standing upright with the carbon atom next to the surface. Again, quantitative comparison between experimental and theoretical curves has been done using the two r-factors r_{ZJ} and r_P.

The interlayer spacing between the C layer and the first bulk layer, $d_\perp$(Ru–C), was varied for the on-top site models between 1.65 and 2.25 Å, for the hollow site models between 0.95 and 2.10 Å, and for the bridge site between 1.10 and 1.70 Å. The C–O bond length was varied between 0.9 and 1.2 Å for the top site and the bridge models only; for the two hollow sites it was kept fixed at 1.15 Å. The step widths in all cases were 0.05 Å. The comparison between the experimental curves and the four model calculations, each one with the parameters which fit best, is shown in fig. 7.

The two hollow site models can be clearly excluded by visual comparison and also by the r-factor analysis. The r-factors are significantly higher than those for the other models, and the two r-factors used here have minima at different interlayer distances. The minimum averaged r-factors for the fcc site are $\bar{r}_P = 0.69$ at $d_\perp$(Ru–C) = 1.80 Å, and $\bar{r}_{ZJ} = 0.38$ at $d_\perp$(Ru–C) = 1.50 Å. The corresponding values for the hcp sites are $r_P = 0.74$ at $d_\perp$(Ru–C) = 1.40 Å and $\bar{r}_{ZJ} = 0.45$ at $d_\perp$(Ru–C) = 1.55 Å.

The comparison of the experimental curves with the calculations for the bridge site and the top site models do not lead to such a clear decision. Visual

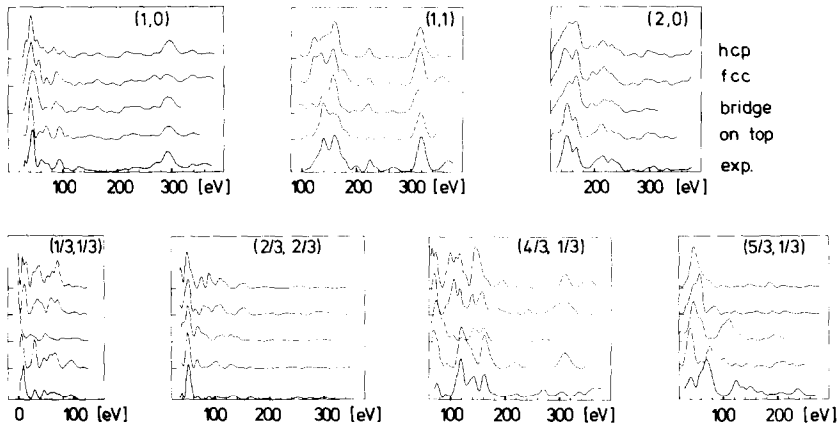

Fig. 7. Comparison of best-fit theoretical $I-V$ curves for (from top) the two threefold hollow sites (hcp site with $d_\perp$(Ru–C) = 1.5 Å, d(C–O) = 1.15 Å, and fcc site with $d_\perp$(Ru–C) = 1.55 Å, d(C–O) = 1.15 Å), the bridge site ($d_\perp$(Ru–C) = 1.3 Å, d(C–O) = 1.10 Å) and the on-top site (d(Ru–C) = 1.95 Å, d(C–O) = 1.1 Å), with the experimental curves (bottom curve in each case) for 7 non-degenerate beams of the $\sqrt{3}$-CO/Ru(001) structure. $V_0 = -12.0$ eV in all models.

comparison leads only to a slight preference for the top site. In the *r*-factor analysis Pendry's *r*-factor gives a clear preference for the top site. The minimum values are $\bar{r}_P = 0.51$ for the top site and $\bar{r}_P = 0.71$ for the bridge site. The corresponding minima for $\bar{r}_{ZJ}$ are 0.26 (bridge) and 0.21 (top site). The difference is smaller but still significant. The minima of the single beam *r*-factors have a wide spread in the Ru–C distance for the bridge site (fig. 8), while for the top site the minima lie close together (see figs. 11 and 12 below). This result is similar to that obtained by Koestner et al. [21] who in a study of CO on Rh(111) also found only slight preferences for the top site compared to the bridge site, when using Zanazzi and Jona's *r*-factor only. Our analysis of both *r*-factors clearly prefers the on-top site.

Having excluded the threefold and bridge sites, we show in detail the optimization for the on-top site. The influence of a variation of the two layer spacings on the calculated *I–V* spectra together with the experimental curves is shown in figs. 9 and 10, and the corresponding *r*-factor plots in figs. 11 and 12. Inspection of these figures shows that visual comparison leads to the same range of optimal parameters as the *r*-factor analysis. Also, it is interesting to note that considerable sensitivity to adsorbate geometry is found in some substrate beams (see the *r*-factors for the (1,0) beam).

The calculations with the same muffin-tin level in all layers exhibit minimum *r*-factors $\bar{r}_P = 0.51$ at d(C–O) = 1.09 Å, d(Ru–C) = 2.00 Å, and $\bar{r}_{ZJ} = 0.21$ at d(C–O) = 1.08 Å and d(Ru–C) = 2.00 Å (where d(Ru–C) and d(C–O), the bond lengths, are identical with the vertical layer distances for this site). Giving the adsorption layers a muffin-tin zero 5.5 eV above that of the Ru layers leads to slightly larger bond lengths, and also to a slight increase of the *r*-factors. The minimum values are here $\bar{r}_P = 0.515$ at d(C–O) = 1.12 Å and d(Ru–C) = 2.05 Å, and $\bar{r}_{ZJ} = 0.23$ at d(C–O) = 1.10 Å and d(Ru–C) = 2.02 Å. An optimization of the muffin-tin zero within the CO overlayer has not been performed since its influence seems to be within the error limits.

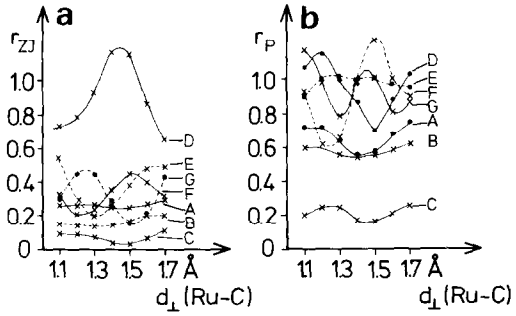

Fig. 8. *r*-factor analysis for the bridge site with (a) r_{ZJ} and (b) r_P as function of the Ru–C layer spacing, d(Ru–C): (A) (1, 0) beam; (B) (1, 1); (C) (2, 0); (D) (1/3, 1/3); (E) (2/3, 2/3); (F) (4/3, 1/3); (G) (5/3, 1/3).

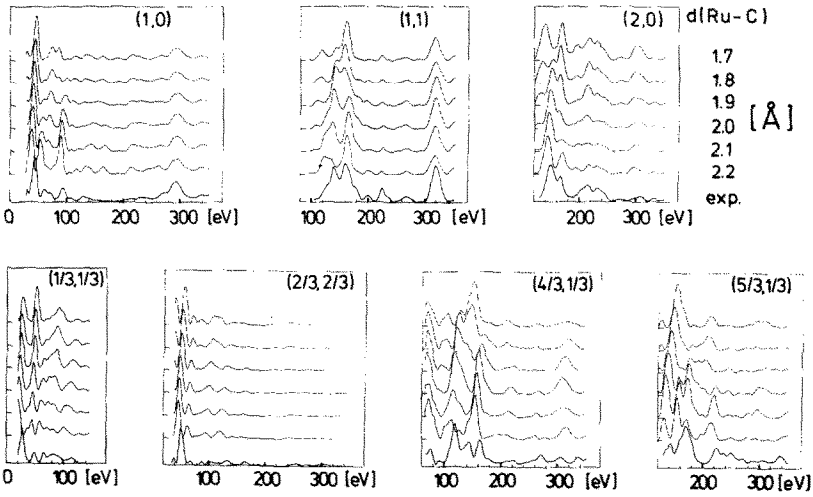

Fig. 9. Comparison of calculated $I-V$ curves for the on-top geometry of $\sqrt{3}$-CO/Ru(001) with different Ru–C distances (from top: d(Ru–C) = 1.7, 1.8, 1.9, 2.0, 2.1 and 2.2 Å; d(C–O) = 1.10 Å and $V_0 = -12.0$ eV in all cases) to experimental curves (bottom curve in all cases) for the indicated beams.

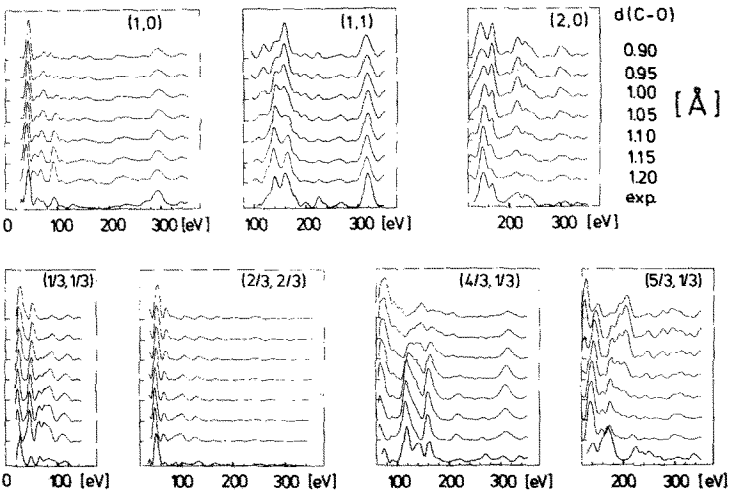

Fig. 10. Comparison of calculated $I-V$ curves for the on-top geometry of $\sqrt{3}$-CO/Ru(001) with different C–O distances (from top: d(C–O) = 0.9, 0.95, 1.0, 1.05, 1.10, 1.15, and 1.20 Å; d(Ru–C) = 1.95 Å, $V_0 = -12.0$ eV in all cases) to experimental curves (bottom curve in all cases), for the indicated beams.

The agreement between the experimental and calculated curves is considerably inferior to that of the clean structure, but comparable to that found for other CO structures. For Pendry's r-factor, which is designed to be metric and independent of the peak heights, a minimum of 0.5 has been found for CO on Ni(100) and 0.4 on Cu(100), respectively [22], and 0.5 on Rh(111) [21]. The relatively low optimum value for Zanazzi and Jona's r-factor found here may be a result of the long energy range of the single beams used in this study. Zanazzi and Jona's r-factor is not metric and not independent of the peak heights. That means it becomes lower at large energies where the $I-V$ curves are strongly damped by the temperature factor.

As can be seen by the elliptic shape of the contour lines in figs. 11 and 12, the C–O and Ru–C bondlengths are strongly correlated, which leads to a large uncertainty of the C position, but rather high accuracy for the Ru–O spacing. This observation has been made previously [21,22]. It has been also pointed out before [21] that the muffin-tin approximation is not a good one for a

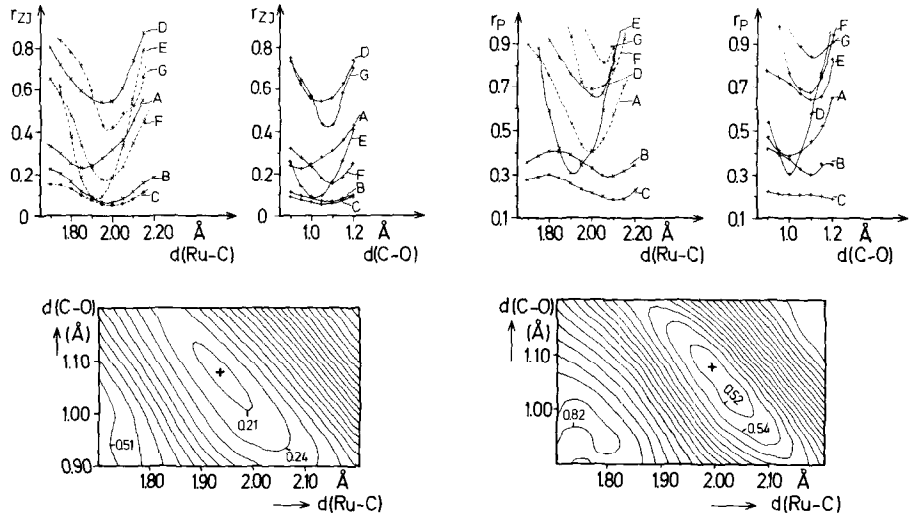

Fig. 11. Optimal fit of the structural parameters of $\sqrt{3}$-CO/Ru(001) in on-top geometry, using the r-factor according to Zanazzi and Jona [25]. Top: variation of d(Ru–C) (left) and d(C–O) (right), for the beams (A) (1, 0), (B) (1, 1), (C) (2, 0), (D) (1/3, 1/3), (E) (2/3, 2/3), (F) (4/3, 1/3), and (G) (5/3, 1/3). Bottom: Contour plot for the all-beam r-factor, $\bar{r}_{ZJ}$, for variation of d(Ru–C) and d(C–O). $V_0 = -12.0$ eV in all cases.

Fig. 12. Optimal fit of the structural parameters of $\sqrt{3}$-CO/Ru(001) in on-top geometry, using the r-factor according to Pendry [26]. Top: variation of d(Ru–C) (left) and d(C–O) (right), for the beams (A) (1, 0), (B) (1, 1), (C) (2, 0), (D) (1/3, 1/3), (E) (2/3, 2/3), (F) (4/3, 1/3), and (G) (5/3, 1/3). Bottom: Contour plot for the all-beam r-factor, $\bar{r}_P$, for variation of d(Ru–C) and d(C–O). $V_0 = -12.0$ eV in all cases.

molecule like CO, and this is probably the reason for the relatively poor agreement between theory and experiment and the remaining large error limits.

We finally conclude a C–O distance of 1.10 ± 0.10 Å and a Ru–C distance of 2.00 ± 0.1 Å, where the error limits are taken from the contour plots of the averaged r-factors assuming an increase by 5% of the r-factor to be significant. The distance Ru–O is, with 3.12 ± 0.02 Å, more accurately known. If we narrow down the range of the coupled d(Ru–C) and d(C–O) by postulating that d(C–O) be not far from 1.15 Å (as suggested by comparison to the CO molecule and to carbonyls [34]), d(Ru–C) becomes about 1.98 Å.

4. Summary and conclusions

The main results of our analysis are

(1) The clean Ru(001) surface is unreconstructed and its first layer spacing slightly contracted as compared to the bulk value ($d = 2.10$ Å instead of 2.14 Å, with an error range of about ± 0.02 Å). For this structure the Zanazzi–Jona r-factor is 0.04, and Pendry's r-factor is 0.16, with an inner potential of -12.0 eV.

(2) The $\sqrt{3}$ structure of CO on Ru(001) consists of molecules in on-top sites in a linear configuration (Ru–C–O), with d(Ru–C) $= 2.0 \pm 0.1$ Å, and d(C–O) $= 1.1 \pm 0.1$ Å. The two distances are correlated, with their sum having much higher accuracy (3.12 ± 0.02 Å). For this geometry the r-factors are $\bar{r}_{ZJ} = 0.21$ and $\bar{r}_P = 0.51$. For the two threefold hollow sites the r-factors are significantly higher; the bridge site gives a similar Zanazzi–Jona r-factor ($\bar{r}_{ZJ} = 0.26$) but a larger Pendry r-factor ($\bar{r}_P = 0.71$).

The finding of a slight contraction for the clean surface is in good agreement with results for other close-packed faces on hcp crystals. For instance, 2% contraction were found on Ti(001) [29], 1% on Zr(001) [32], and layer spacings very close to the bulk were reported for Co(001) [28], and Sc(001) [33].

The structure found for the adsorbed CO is in agreement with the expectations from other methods such as angle-resolved UPS [5], vibrational spectroscopy [7,8], ESD [9], and ESDIAD [10]. It also compares well with the data for ruthenium carbonyls and for other adsorbed CO in on-top sites. In various Ru carbonyls, the Ru–C distance for singly coordinated CO lies between 1.83 and 1.98 Å; the C–O distance is found between 1.13 and 1.22 Å [34]. Compared to these, our distances are on the short side of these ranges for C–O, and on the long side for Ru–C, which may be partly caused by the observed compensation. CO adsorbed in on-top sites has been investigated by LEED on Ni(100) [20,22,35], Cu(100) [22], Pd(100) [36], and Rh(111) [21]. The metal–C distances were determined as 1.72 (Ni), 1.90 (Cu), 1.93 (Pd), and 1.95 (Rh) Å. As expected, our value is close to those of Pd and Rh, its neighbours in the periodic table (the similar bond on Ni is probably shorter because of the

smaller atomic radius; the similar d value on Cu is due to the weak bond). The C–O distance is found as 1.13 to 1.15 Å in all cases except on Rh, where it is given as 1.07 Å; in good agreement with our value. It is seen that all aspects of our results compare well with expectation. Together with the rather acceptable r-factors, we take this as proof of the basic correctness of our findings.

Acknowledgement

This work is a collaborative effort of Sonderforschungsbereich 128 and has been supported by the Deutsche Forschungsgemeinschaft.

References

[1] T.E. Madey and D. Menzel, Japan. J. Appl. Phys. Suppl. 2, Part 2 (1974) 229.
[2] H. Pfnür, P. Feulner, H.A. Engelhardt and D. Menzel, Chem. Phys. Letters 59 (1978) 481.
[3] H. Pfnür and D. Menzel, J. Chem. Phys., in press.
[4] J.C. Fuggle, T.E. Madey, M. Steinkilberg and D. Menzel, Surface Sci. 52 (1975) 521.
[5] M. Steinkilberg, J.C. Fuggle and D. Menzel, Chem. Phys. 11 (1975) 307.
[6] R. Hesse, P. Staib and D. Menzel, Appl. Phys. 18 (1978) 227.
[7] G.E. Thomas and W.H. Weinberg, J. Chem. Phys. 70 (1979) 1437.
[8] H. Pfnür, D. Menzel, F.M. Hoffmann, A. Ortega and A.M. Bradshaw, Surface Sci. 93 (1980) 431.
[9] P. Feulner, H.A. Engelhardt and D. Menzel, Appl. Phys. 15 (1978) 355;
J.C. Fuggle, E. Umbach, P. Feulner and D. Menzel, Surface Sci. 64 (1977) 69.
[10] T.E. Madey, Surface Sci. 79 (1979) 575.
[11] E.D. Williams, W.H. Weinberg and A.C. Sobrero, J. Chem. Phys. 76 (1982) 1150.
[12] H. Pfnür and D. Menzel, Verhandl. Deut. Physik. Ges. (VI) 16 (1981) 977;
H. Pfnür and D. Menzel, to be published;
H. Pfnür, Thesis, TU München (1982);
D. Menzel, H. Pfnür and P. Feulner, Surface Sci. 126 (1983) 374.
[13] E.D. Williams and W.H. Weinberg, Surface Sci. 82 (1979) 93.
[14] H.A. Engelhardt, P. Feulner, H. Pfnür and D. Menzel, J. Phys. E10 (1977) 1133.
[15] P. Feulner, Thesis, TU München (1981);
P. Feulner and D. Menzel, to be published.
[16] G. Michalk, Diplom-thesis, TU München (1981).
[17] J.B. Pendry, Low Energy Electron Diffraction (Academic Press, London, 1975).
[18] K. Schwarz, Theoret. Chim. Acta (Berlin) 34 (1975) 225.
[19] R. Feder and W. Moritz, Surface Sci. 77 (1978) 505.
[20] S.Y. Tong, A. Maldonado, C.H. Li and M.A. Van Hove, Surface Sci. 94 (1980) 73.
[21] R.J. Koestner, M.A. Van Hove and G.A. Somorjai, Surface Sci. 107 (1981) 439.
[22] S. Andersson and J.B. Pendry, J. Phys. C13 (1980) 3547; Phys. Rev. Letters 43 (1979) 363.
[23] International Tables for X-Ray Crystallography, Vol. III (Kynoch, Birmingham, 1962).
[24] H.B. Nielsen and D.L. Adams, J. Phys. C15 (1982) 615.
[25] E. Zanazzi and F. Jona, Surface Sci. 62 (1977) 61.
[26] J.B. Pendry, J. Phys. C13 (1980) 937.
[27] R.S. Zimmer, Surface Sci. 43 (1974) 61.

[28] G.L.P. Berning, Surface Sci. 61 (1976) 673; 104 (1981) L225.
[29] H.D. Shih, F. Jona, D.W. Jepsen and P.M. Marcus, J. Phys. C9 (1976) 1405.
[30] J. Jagodzinski, Z. Naturforsch. 37a (1982) 1103.
[31] H. Pfnür, Thesis, TU München (1982);
H. Pfnür and D. Menzel, to be published.
[32] W.T. Moore, P.R. Watson and D.C. Frost, J. Phys. C12 (1979) L887.
[33] S. Tougaard, A. Ignatiev and D.L. Adams, in: Proc. 4th Intern. Conf. on Solid Surfaces, Cannes, 1980, Eds. D.A. Degras and M. Costa (Paris, 1980) p. 677.
[34] S.C. Tripathi, S.C. Srivastava, R.P. Mani and A.K. Shrimal, Inorg. Chim. Acta 15 (1975) 249.
[35] M. Passler, A. Ignatiev, F. Jona, D.W. Jepsen and P.M. Marcus, Phys. Rev. Letters 43 (1979) 360.
[36] R.J. Behm, K. Christmann, G. Ertl, M.A. Van Hove, P.A. Thiel and W.H. Weinberg, Surface Sci. 88 (1979) 259.